Mediterranean Marine Science

Vol 18, No 1 (2017)

Comparison of high resolution hydrodynamic model outputs with in-situ Argo profiles in the Ionian Sea

D. KASSIS, G. KORRES, A. KONSTANTINIDOU, L. PERIVOLIOTIS

doi: 10.12681/mms.1753

Research Article

Mediterranean Marine Science
Indexed in WoS (Web of Science, ISI Thomson) and SCOPUS
The journal is available on line at http://www.medit-mar-sc.net
DOI: http://dx.doi.org/10.12681/mms.1753

Comparison of high resolution hydrodynamic model outputs with *in-situ* Argo profiles in the Ionian Sea

D. KASSIS[1,2], G. KORRES[1], A. KONSTANTINIDOU[1] and L. PERIVOLIOTIS[1]

[1] Institute of Oceanography, Hellenic Centre for Marine Research, PO Box 712 Anavyssos, 190 13, Greece
[2] Department of Naval Architecture and Marine Engineering, National Technical University of Athens, Heroon Polytechniou 9, Athens 15773, Greece

Corresponding author: dkassis@hcmr.gr

Handling Editor: Takvor Soukissian

Received: 25 March 2016; Accepted: 3 October 2016; Published on line: 3 February 2017

Abstract

In-situ monitoring is an essential component for the development of hydrodynamic numerical models. Argo expansion into marginal seas has enabled the advancement of high resolution regional nested models through initialization, assimilation and validation processes. The SANI (Southern Adriatic-Northern Ionian) hydrodynamic model is a regional nested model producing high resolution outputs for the period 2008-2012. For the corresponding time period, 21 free drifting Argo floats recorded Temperature –Salinity (T/S) profiles throughout the region. This study presents the inter-comparison of the two data sets whilst noting interesting aspects of the model performance regarding the representation of the major water masses characteristics of the SANI area mainly focusing on the Ionian region. Aside from the inter-comparison in a basin's scale, a spatio-temporal analysis is also performed. The results indicate an adequate response of the model simulations regarding the basic hydrographic features of the region. Nevertheless, important differences are highlighted mainly in the upper and deep layers of the study area. At a regional scale, inter-annual variability of the model's performance is observed reflecting the hydrographic changes occurred in the wider area during the study period. Overall, the results present the strong points but also highlight the weaknesses of the model. They also confirm the challenging task of producing high resolution numerical simulations in transitional areas such as the Ionian and Adriatic Seas.

Keywords: Argo floats, hydrodynamic forecasting, temperature profiles, salinity profiles.

Introduction

Throughout the last decade, operational oceanographic activities have expanded in regional seas. Hydrodynamic simulations now provide more information, and datasets of higher resolution and quality than ever before. This enhanced capability is mainly due to the advancement of in-situ monitoring tools. The Argo array, a multi-national fleet of autonomous free-drifting profilers, is one such tool used for the initialization, assimilation, and assessment of numerical models (Tonani *et al.,*, 2014). In regards to the Mediterranean Sea, the coverage of Argo profilers gradually expands through the combined efforts of the newly formed Euro-Argo European Research Infrastructure (EuroArgo ERIC) (www.euro-argo.eu), national initiatives and the coordination of MedArgo (http://nettuno.ogs.trieste.it/sire/medargo). Increasing numbers of Argo profiles in enclosed basins and coastal areas have enabled the development of high resolution modelling through the validation of nested regional models. Such is the SANI (Southern Adriatic-Northern Ionian) hydrodynamic model that has provided high spatial resolution output data for a time period of five years (2008-2012). SANI model has been developed for the IONIO INTERREG-III project and has been integrated as an additional component into the POSEIDON ocean forecasting system (http://poseidon.hcmr.gr) producing forecasts for the Northern Ionian and the South Adriatic Seas. The latter system is composed of the Mediterranean (~ 10 km resolution) hydrodynamic and wind-waves models along with nested models that downscale the basin scale solution up to the resolution of approximately 3 km in the Aegean and the eastern flank of the Ionian Seas (Nittis *et al.,* 2006; Korres *et al.,* 2009). Poseidon is also accompanied with a numerical weather prediction system based on ETA non-hydrostatic atmospheric model which provides 5-days forecasts at ~ 5 km resolution over the Mediterranean Sea (Papadopoulos and Katsafados 2009).

In this work we focus on the Ionian region, an area that has undergone changes regarding its hydrography during the period of study (Gačić *et al.,* 2010; Bensi *et al.,* 2013; Velaoras *et al.,* 2013; Kassis *et al.,* 2013; Theocharis *et al.,* 2014; Gačić *et al.,* 2014). The conditions of the Ionian Sea make it an important region for obtaining high resolution hydrodynamic data. It fills the deepest basin in the Mediterranean and is a transitional area where water masses from Western and Eastern Mediterranean meet and interact (Nittis *et al.,* 1993; Lykousis *et al.,* 2015). Covering a surface area of

more than 200.000 km^2 and reaching depths of 4800 m, the Ionian Sea has been the study target of many research activities in the past which have highlighted the role of the sub-basin on the wider area (Theocharis *et al.,* 1993; Nittis *et al.,* 1993; Gacic *et al.,* 1996; Roether *et al.,* 1996; Malanotte-Rizzoli *et al.,* 1997). The Sicily Straits create a pathway from the Western to Eastern Mediterranean basin. The Ionian Sea also communicates with a number of semi-enclosed sub-basins of the Eastern Mediterranean, where distinct water masses are formed, such as the Levantine (through Libyan Sea) from the south, the Aegean from the south-east (Antikithira Straits) and the Adriatic from the north (Otranto Strait).

Here we present an assessment of SANI simulations through the inter-comparison of the model's temperature-salinity (T-S) profiles with the T-S profiles of 21 Argo floats operating within the region during the 5-years (2008-2012) period. Model validity, regarding the representation of major water mass characteristics is discussed at a regional and basin level. Furthermore we investigate the model's efficiency regarding interannual and seasonal hydrographic changes of the area.

The paper is organized as follows. "Materials and Methods" section describes the existing knowledge for the study area, the characteristics of the SANI model, the Argo floats configuration and the methods used for the data analysis. The "Results" section presents the outputs of the inter-comparison in regional, annual, seasonal and overall averaged scale. Finally in the "Discussion" section the results and conclusions are summarized together with the future upgrades of the SANI model.

Materials and Methods

Study area

The Ionian Sea covers an extended area both in surface and in depth (Fig. 1A, 1B). The basin's interconnectivity plays a key role in controlling the multiannual variability of the whole Eastern Mediterranean Sea. The typical water masses that dominate the Ionian's surface and sub-surface layers are the Levantine Surface Water (LSW), the Ionian Surface Water (ISW), and the Atlantic Water (AW). The AW moves eastward through the Sicily Straits, it is characterized by a salinity minimum, and is clearly distinguished from the saltier and warmer ISW and the salinity maximum of the LSW. In the intermediate layer, at depths varying between 100 and 500 m, another water mass of Levantine origin, the Levantine Intermediate Water (LIW) is clearly associated with another salinity maximum. In the same depth horizon, the Cretan Intermediate Water (CIW) is slightly denser than LIW, and enters the Ionian from the Aegean basin. The deeper layers of the Ionian basin are occupied by the so-called Transitional Waters (TW) (500-1200m) and the Eastern Mediterranean Deep Waters (EMDW) filling the layers below 1200m (Nittis *et al.,* 1993; Malanotte-Rizzoli *et al.,* 1997). Additionally, two regionally confined water masses, the Cretan Deep Water (CDW) of Aegean origin and the Adriatic Deep Water (AdDW), being both the result of deep water formation events, fill the deeper layers of the area. Thus, EMDW has transitional characteristics since it is a mixture of CDW, AdDW and other water masses (Hainbucher *et al.,* 2014).

The hydrography of the Ionian basin is controlled by both internal and external mechanisms and changes. At

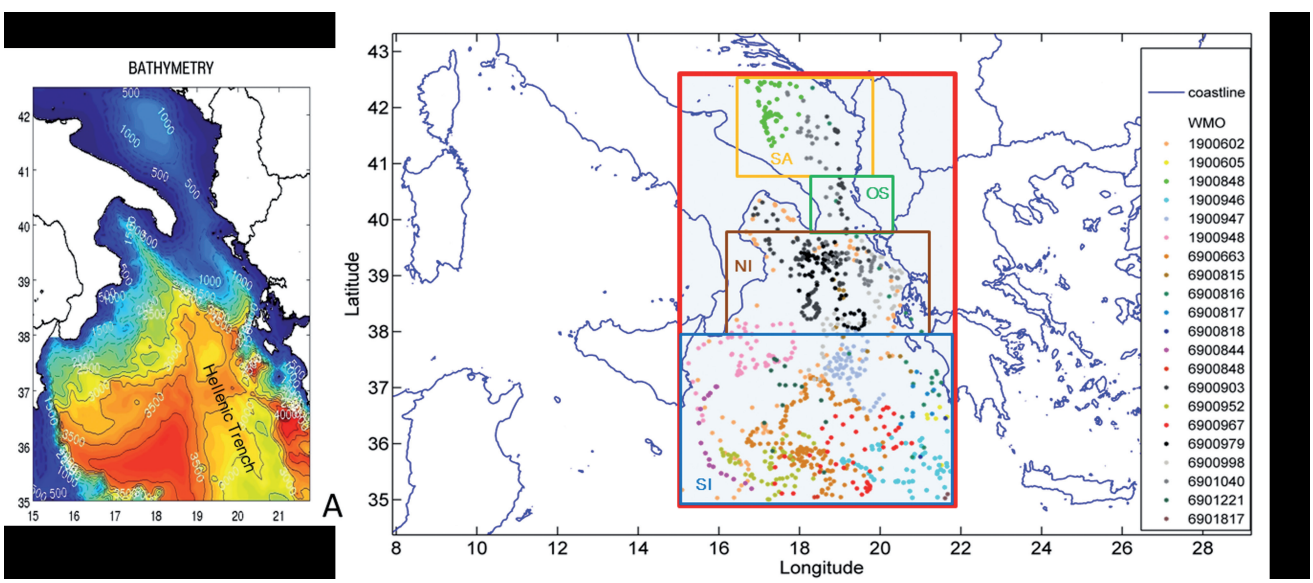

Fig. 1: SANI model bathymetry (A). The geographical area covered by SANI model (red rectangular) and the divided sub-regions SA (Southern Adiatic - yellow), OS (Otranto Strait - green), NI (Northern Ionian – brown) and SI (Southern Ionian – blue). All the available (966) Argo profiles for the period 2008-2012 from 21 individual floats denoted with different colours according to their WMO number (B).

the end of the 80's, researchers focused on the Ionian as an area being directly affected by the drastic change in the eastern Mediterranean named as the Eastern Mediterranean Transient (EMT) (Roether and Schlitzer 1991; Theocharis *et al.,* 1993; Roether *et al.,* 1996; Malanotte-Rizzoli *et al.,* 1997; Theocharis *et al.,* 2002; Klein *et al.,* 2000). Dense waters that were produced in the Aegean filled the deep layers of the Ionian basin lifting the isopycnals by hundreds of meters (Klein *et al.,* 1999). Towards the end of the 90's, the Ionian's general upper circulation changed from anticyclonic to cyclonic. There were suggestions that such a reversal was mainly wind driven (Pinardi *et al.,* 2015), while other studies related this change to EMT relaxation (Borzelli *et al.,* 2009). Following this, a feedback mechanism between the Ionian basin and the southern Adriatic was introduced (Gačić *et al.,* 2010) named as BiOS (Adriatic–Ionian Bimodal Oscillating System). According to the above mechanism, the Ionian-Adriatic interaction is associated to an almost decadal thermohaline oscillation characterized by the alternation of a cyclonic to anti-cyclonic circulation of the Ionian upper layers. This procedure has also been connected with the role of the Aegean Sea acting as a source for dense water formation (Theocharis *et al.,* 2014). Thus during the cyclonic phase, the Aegean Sea becomes preconditioned for dense water formation due to an increase of the surface salinity in the Levantine. On the contrary, during the anti-cyclonic phase, the Adriatic Sea enters the preconditioned status (Gačić *et al.,* 2010; Meccia *et al.,* 2015).

During the period of our study (2008-2012), three inversions in the Ionian upper layers circulation have been identified. The anticyclonic mode dominated during 2008-2010 period, while a reversion to cyclonic mode occurred in 2011 (Bessières *et al.,* 2013; Gačić *et al.,* 2014). Nevertheless a new anti-cyclonic reversion occurred during 2012 that was associated with the extreme winter conditions in the Adriatic during this year. This resulted in the formation of very dense water in the Adriatic that flooded the Northern Ionian during May 2012 (Gačić *et al.,* 2014). Furthermore, at the south-eastern part of the basin, dense water outflow has been recorded during 2009 from the Aegean Sea, that followed a northward path along the Hellenic Trench giving a signal of increased salinity in the intermediate layers (Kassis *et al.,* 2013). This outflow was the result of the preconditioned for dense water formation status of the Aegean that has been reported for the period 2007-2012 (Schroeder *et al.,* 2013; Krokos *et al.,* 2014; Cardin *et al.,* 2015; Kassis *et al.,* 2015) and resulted in the alternation of the south-eastern Ionian upper and intermediate waters. The aforementioned short term inter-annual changes in the area's hydrography create a challenging field for the performance of numerical hydrodynamic simulations.

Hydrodynamic model

The numerical circulation SANI model is a hydrodynamic model that is based on Princeton Ocean model (POM), a primitive equations free surface ocean model which operates under the hydrostatic and Boussinesq approximations. The model equations are written in sigma-coordinates and discretized using the centered second-order finite differences approximation in a staggered "Arakawa C-grid" with a numerical scheme that conserves mass and energy. POM uses two sub-models for the computation of the eddy mixing (second order turbulence closure scheme–Mellor & Yamada 1982) and horizontal non-linear viscosity. It also uses a time splitting technique for the external (barotropic) and internal (baroclinic) modes. The modelling system operates at a high spatial resolution of 1/50° x 1/50° in horizontal (approximately 2.5 x 2.5 km) and 25 sigma-layers along the vertical with a logarithmic distribution near the surface and the bottom. The model covers the geographical area 15° E - 21.76° E & 35° N - 42.5° N (Fig. 1A, 1B) and its bathymetry has been obtained from the US Navy Digital Bathymetric Data Base – DBDB1 – (with a nominal resolution of 1/60º x 1/60º) by bilinear interpolation. The model includes parameterization of five Albanian (Drin, Mat, Semani, Vjosa, Erzen) and one Greek river (Acheloos) using monthly outflow values from 1990 – 2000 climatology (Ludwig 2007). The model runs on a daily basis (initialized at 00:00 UTC) and produces 24-hour simulations at hindcast mode and 5-day simulations at forecast mode. It is forced with surface hourly fluxes of momentum, heat and freshwater from the Poseidon - ETA atmospheric model either directly (short-wave radiation, downward longwave radiation, freshwater flux) or through a properly tuned set of bulk formulae utilizing atmospheric parameters and the SANI model predicted SST (turbulent and momentum fluxes, upward longwave radiation). In particular, the net shortwave radiative gain received by the ocean at the sea surface is calculated by the ETA model using an advanced radiative transfer algorithm which takes into account the vertical structure of the atmospheric column (Saharian dust effect, etc.) and is provided then directly to the hydrodynamic model at hourly intervals. Part of the shortwave radiative gain is absorbed at the sea surface while the remainder is directly added to the heat equation following Jerlov (Jerlov 1976) attenuation function for clear water. The same approach (direct input by the atmospheric model) is followed for the downward atmospheric infrared radiation reaching the sea surface while the upward infrared radiation flux emitted by the ocean is calculated at each time step by the hydrodynamic model using the Stefan-Boltzman law and the model's SST. The turbulent heat fluxes at the sea surface (evaporative and sensible heat flux) are calculated by the SANI system itself using bulk aerodynamic formulae, the model simulated SST and the atmospheric pa-

rameters of 10m wind speed, air temperature and relative humidity (at 2-meters) as provided by the ETA model. The turbulent exchange coefficients used in the bulk formulae are calculated using the Kondo scheme. As for the momentum flux boundary condition, the calculation of the wind stress fields at the air-sea interface is based on the 10m wind speed of the ETA model and the drag coefficient calculated according to the Hellerman and Rosenstein (1983) polynomial approximation.

The SANI modelling system has been integrated in hindcast mode for a 5 years period (2008-2012) forced with the POSEIDON/Eta analyses and nested within the MyOcean MFS model.

As already said, lateral boundary conditions at the four open boundaries of SANI model are provided on a daily basis (daily averaged fields) by the MFS - MyOcean model (Oddo *et al.,* 2009) covering the whole Mediterranean Sea with a resolution of 1/16^{o} and 71 unevenly spaced vertical levels. The off-line nesting between the two models involves the zonal/meridional external (barotropic) and internal velocity components, the temperature/salinity profiles and the free surface elevation following the nesting procedures described by Korres and Lascaratos (2003).

To benefit from the data assimilation of satellite Sea Level Anomaly (SLA), SST and in-situ Argo float profiles that takes place on a weekly basis in the MFS system, SANI was periodically (weekly) re-initialized from the MFS model results namely 2D free surface elevation and 3D velocities, temperature and salinity fields mapped via interpolation techniques to the SANI model domain. In order to filter out spurious oscillations that may occur during the re-initialization procedure, the VIFOP optimization tool (Auclair *et al.,* 2006) has been implemented in the forecasting system. VIFOP is a variational initialization technique based on the minimization of a cost function involving data constraints as well as a dynamical penalty involving the tangent linear model. The spurious oscillations affect mainly the barotropic variables of the model (depth integrated velocities and free surface elevation) contaminating the model forecasts and can be efficiently suppressed in magnitude and duration by optimizing the global divergence of the external mode and the free surface tendency and by using the strong constraint on the free surface tendency.

In this work, the period of the comparison of the SANI model temperatures and salinities against Argo temperature and salinity profiles is January 2008 to December 2012.

Argo floats

The majority of the free-drift profiling floats in Mediterranean are configured according to the MedArgo specifications (Poulain *et al.,* 2007). This requires 5-days drifting cycles at 350 m depth while the profiling depth is set to 1000 m. Nevertheless a number of older floats in the area were programmed according to International Argo specifications. These floats drift at 1000 m depth and descend to 2000 m in order to acquire the ascending profile in continuous 10-day cycles. All the profilers are equipped with the standard CTD sensors SBE 41/41CP pumped MicroCAT (www.seabird.com/products/ArgoCTDandFloat.htm) with accuracies of 0.002 oC, 0.005 psu and 2.4 dbars for temperature, salinity and pressure respectively. All Argo T/S profiles associated with the study area and time period of study were examined. The profiles were acquired from the Coriolis Data Assembly Centre (www.coriolis.eu.org/Observing-the-Ocean/ARGO) and only the values flagged as "good" after the automatic quality control procedure were used. The acquired profiles were 966 from a fleet of 21 floats (Fig. 1A) and generally characterized as good quality (<1.8% flagged as dubious values). Less than 6% of the values were missing, however the majority of those were surface salinity data. An apparent increase of the Argo profiles over time (42 profiles during 2008, 69 during 2009, 162 during 2010, 217 during 2011 and 476 during 2012) reflects the increased deployments activity in the area during this period. Additionally, the profiles have been validated through a delayed mode visual check. This resulted in a sub-set of 946 valid profiles within the geographical area that SANI covers for the period 2008-2012. Each Argo profile was co-located with an associated model output. The final Argo and model datasets are linearly interpolated to the same depth levels (0:10:1000 m) for their inter-comparison. The associated model and Argo profiles are classified into 4 geographical regions in order to study spatial differences between the two datasets. These regions are: 1. Southern Adriatic (SA), Otranto Strait (OS), Northern Ionian (NI) and Southern Ionian (SI) (Fig. 1B). Furthermore, a temporal classification is made in order to identify inter-annual and seasonal patterns of the inter-comparison. According to this, the profiles are separated into 5 sub-sets of consequent years (Table 1) and divided into two seasonal semesters that represent: 1. the "winter" period of deep mixing (384 profiles between November – April) and 2. the "summer" period of intense stratification (562 profiles between May – October).

Results

Regional analysis

For the regional analysis, we present the averaged T/S profiles and their standard deviation from the Argo and model datasets together with the - over time - Hovmöller diagrams of the differences from the profile to profile comparisons. In the seasonal analysis, we present the averaged T/S from both datasets for the "winter" and "summer" periods within the first 200 m in order to examine models performance in the cases of surface cooling and heating respectively. For the general results, we present the averaged profiles of the whole study area,

their differences, and the T-S diagram of all the profiles for intermediate and deep waters. Furthermore the Root Mean Square Errors (RMSE) profiles and the residuals for each profile couple at 6 discrete depths are plotted.

Since the number of profiles differs in each sub-domain (Table 1), a statistical analysis was performed in order to quantify the statistical significance of the mean differences with depth for both temperature and salinity. A two independent samples t-test has been applied through which the ***t*** statistic value was calculated according to the formula:

$$t = \frac{M_A - M_m}{\sqrt{\frac{S_A{}^2 + S_m{}^2}{N}}}$$

Where N is the number of profiles in each sub-domain, M_A and M_m are the Argo and model means for each depth level and S_A, S_m their standard deviations accordingly. For each sub-domain and depth level, the null-hypothesis has been tested against the alternative hypothesis. The null hypothesis assumes that the samples come from populations with equal means and thus any calculated Argo-model difference cannot be safely assigned to model's performance. The alternative hypothesis indicates that the means are unequal and therefore the Argo-Model differences are systematic, allowing us to draw conclusions regarding model's efficiency. Additionally, the value p, representing the probability, under the null hypothesis, of observing a value as extreme or more extreme of t, has been calculated. The null hypothesis can be rejected when $p < 0.05$ indicating that the mean of the Argo-Model differences, at that specific depth level, does not become 0 at a confidence interval of 95%. The statistical significance of the differences varies with depth in each sub-domain (Fig. 2), whilst the number of the available profiles N is proved to be crucial for the rejection of the null hypothesis at the 0.05 significance level. Thus, for the Northern and Southern Ionian sub-domains the Argo-model temperature differences are statistically significant at a confidence level of approximately 99% in almost every depth layer (Fig. 2B). Regarding salinity there are differences at specific depth layers where p is high (> 0.05) and thus the null-hypothesis cannot be rejected (Fig. 2D). For the Southern Adriatic and Otranto Strait sub-domains (Fig. 2A, 2C) the depth layers of low confidence interval (high p) are more extended for both T and S mean differences. This is related with the small number of available profiles in these areas (Table 1). For that reason, the results presented from these two sub-domains are only indicative and more profile comparisons are needed in order to draw safe conclusions. The whole area (Fig. 2E) follows a similar distribution with Ionian sub-domains. Temperature differences are presented significant in the whole water column whilst for salinity only at narrow depth layers the null-hypothesis is rejected (20 – 30 m, 190 – 200 m and 700 – 780 m) (Fig. 2E).

Southern Adriatic

In the southern Adriatic area the available profiles correspond to the years 2010 and 2012 (Fig.3C, 3D). Regarding temperature, the model presents a systematic underestimation compared to the Argo profiles at the surface layers (0-50 m) ranging from 0.1 to 4.6 °C (Fig. 3C). Deeper than 50 m, this figure remains constant until 850 m where temperature differences become negligible (< 0.01 °C). Nevertheless, several profiles exhibit slight overestimations of the model at sub-surface and intermediate depths for temperature (Fig. 3C).

Regarding salinity, the model also presents an underestimation on average from the surface down to 800 m depth (Fig. 3B). At the surface layers the average underestimation is 0.04 psu and reaches a maximum of 0.055 psu at the signal of the LIW core (180 - 190 m). Inter-annual differences are apparent for salinity values in the surface and sub-surface layers, thus, during 2010, the model predicts "saltier" waters than the in-situ data records, whilst model runs in 2012 predict "fresher" waters than Argo data (Fig. 3D). For depths below 200 m, the in-situ average profile presents a constant salinity field (38.705-38.720), whilst the averaged model output presents a gradual increase from 38.65 to 38.74 at 1150 m depth. The salinity overestimation of the deep profiles of 2010 from the model results in the overestimation of the AdDW's salt content (Fig. 3B, 3D).

The temperature standard deviation (STD) is higher for both Argo and model profiles in the upper layers (approximately ± 1 °C) reflecting the high variability of these layers due to surface heat exchanges (Fig. 3A). Regarding salinity, Argo STD is presented as higher than the model's, especially at subsurface and intermediate layers. This fact reflects a high tempo-spatial variability of the salt content that was recorded by the floats which is not apparent in the model's results (Fig. 3B).

Otranto Strait

23 Argo-model profiles were analysed in the Otranto Strait region corresponding to four consecutive years (2009-2012). At certain depths, differences between the model outputs and the in-situ Argo measurements vary inter-annually for both temperature and salinity (Fig. 4C, 4D). At surface layers the model generally indicates an underestimation of both temperature and salinity values with the exception of salinity values calculated for 2011 where model's salinity appears greater than the salinity measured by Argo floats. As a general rule, at depths below 100m, temperature is underestimated by the model for all the years. Regarding salinity, a similar pattern is shown at the intermediate layers for 2009, 2010 and 2012; however, 2011 indicates both positive and negative differences between the two data sets (Fig 4C, 4D). Comparing the average profiles for the two datasets (Fig. 4A, 4B), similar patterns to those depicted in the southern Adriatic region appear,

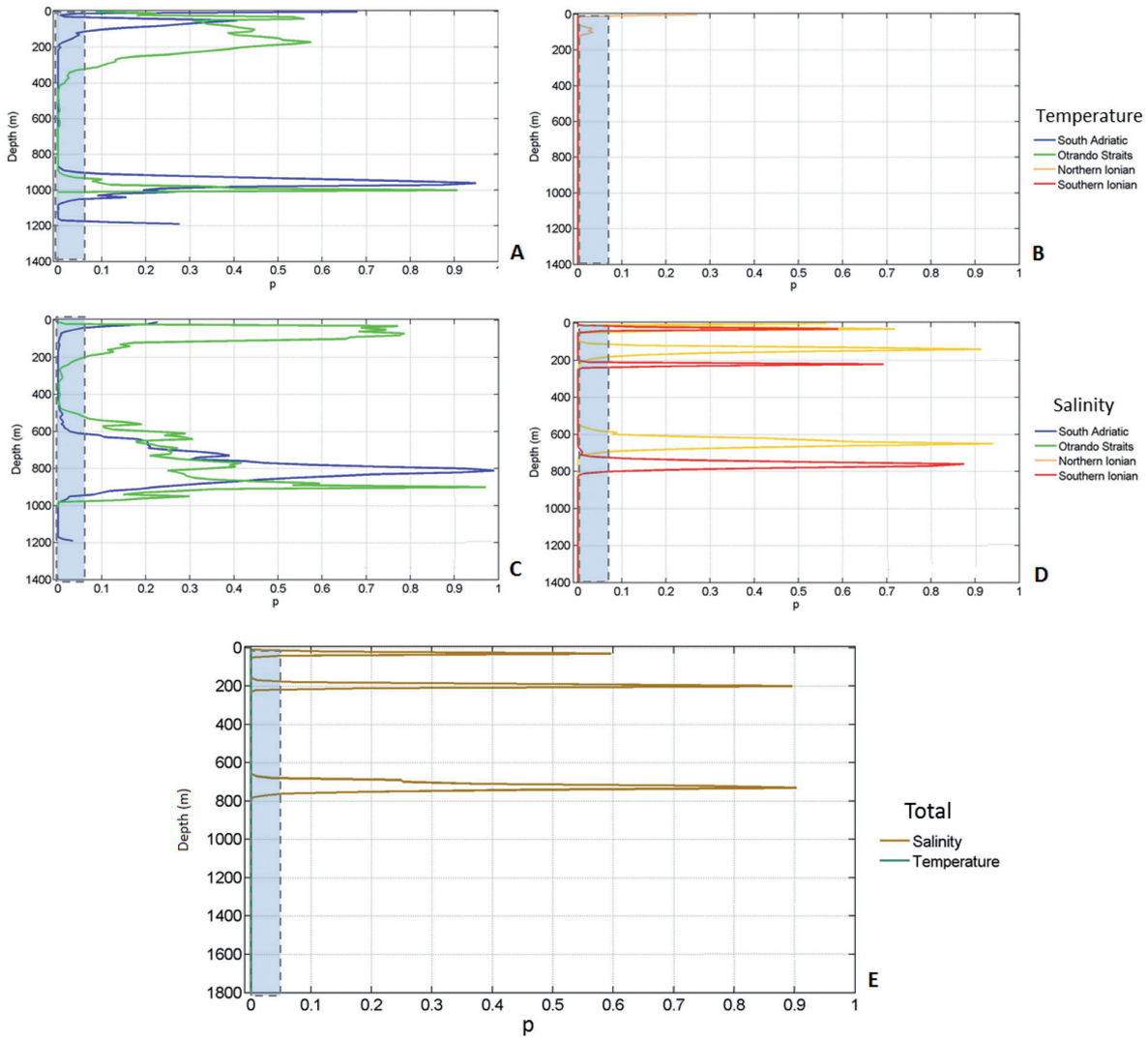

Fig. 2: **A:** Confidence level along depth for Argo-model average temperature profile differences in South Adriatic (blue) & Otranto Strait (green). **B:** Confidence level along depth for Argo-model average temperature profile differences in Northern (yellow) and Southern (red) Ionian. **C:** Confidence level along depth for Argo-model average salinity profile differences in South Adriatic (blue) & Otranto Strait (green). **D:** Confidence level along depth for Argo-model average salinity profile differences in Northern (yellow) and Southern (red) Ionian. **E:** Confidence level along depth for Argo-model average temperature (green) and salinity (brown) profile differences in the whole study area. The shaded rectangular denotes the area of statistical significant differences with a confidence of 95% between the Argo and model distributions (null-hypothesis rejected, $p < 0.05$).

i.e. model underestimation at surface waters with the opposite occurring at deeper depths. The AW core is apparent in the Argo salinity average profile at approximately 50 m, whilst the LIW core (38.85 - 38.87 psu) is present in the layer between 150 and 300 m (Fig. 4B). The model presents salinity average underestimation of 0.5 psu in this layer, whilst it seems to underestimate salinity during all years apart from 2011 (Fig. 4D). On the contrary, it overestimates the salinity of the cold and fresher water shown from Argo profiles near 1000 m which represents AdDW (Fig. 4D).

The levels of STD are similar to Southern Adriatic, however the differences in the salinity STD that are less prominent here (Fig. 4B).

Northern Ionian

For the Northern Ionian region, the majority of available profiles are taken during 2012 (Table 1). At surface layers, there is a general underestimation of temperature by the model which, in cases, reaches up to 6.7 ^{o}C. In the deep layers (> 600 m) the profile to profile comparison shows a slight but constant temperature underestimation whilst at intermediate depths the temperature differences present a much more variable behaviour (Fig. 5C). According to this, Argo-model differences are depicted either slightly negative or strongly positive. Nevertheless, the temperature averaged profiles over all years indicate a slight underestimation of the model's temperature that starts below 100 m and increases gradually to reach 0.36 ^{o} C at the maximum depth of over 1000 m (Fig. 5A).

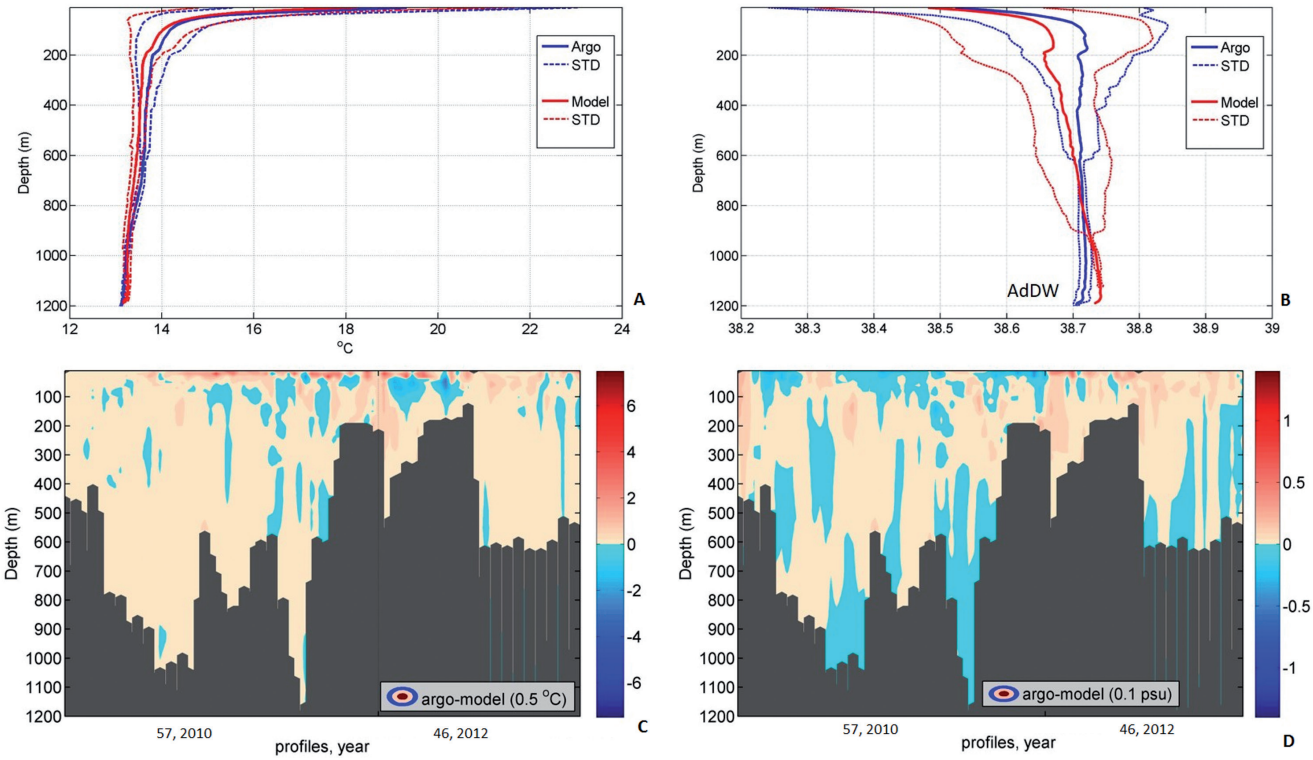

Fig. 3: Temperature (A) and salinity (B) average profiles with the associated STD for model (red) and Argo (blue), calculated from the available profiles in the southern Adriatic region. Hovmöller diagrams of the differences between Argo and model associated profiles over time for temperature (C) and salinity (D) in the south Adriatic.

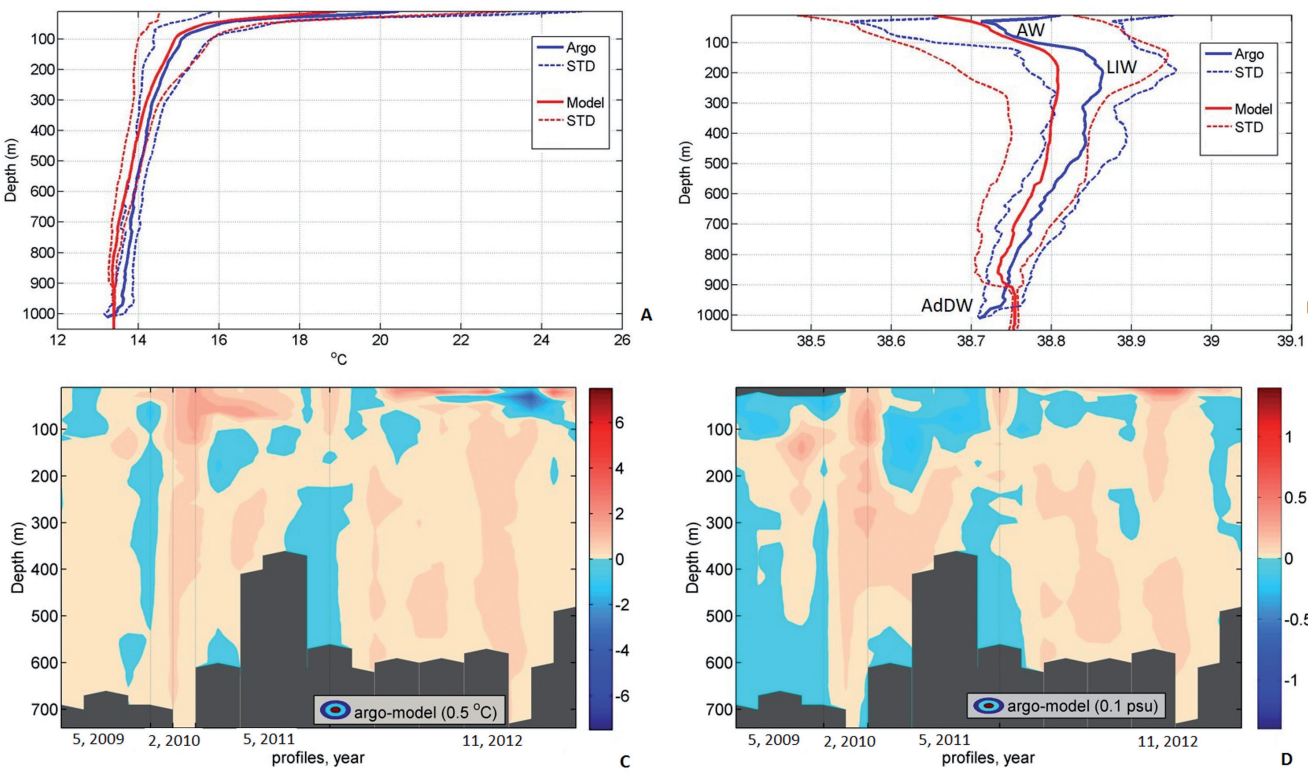

Fig. 4: Temperature (A) and salinity (B) average profiles with the associated STD for model (red) and Argo (blue), calculated from the available profiles in the Otranto Strait. Hovmöller diagrams of the differences between Argo and model associated profiles over time for temperature (C) and salinity (D) in the Otranto Strait.

Regarding salinity profiles, the differences between the model outputs and Argo measurements show that in deep water (> 600 m), salinity seems to be overestimated by the model (Fig. 5D). Comparison of the average profiles of both data sets shows an underestimation of the model at both surface layers and at the LIW core (180-400 m) (Fig. 5B). At 50 m, the AW signal is presented "saltier" by the model in comparison to the Argo data (38.79 vs. 38.75 psu), while at the deeper layers (800-1600 m), the model also overestimates salinity by 0.02-0.03 psu (Fig. 5B).

For both temperature and salinity STDs are significantly less than the previous two sub-domains whilst there is no significant difference between Argo and model profiles (Fig. 5A, 5B).

Southern Ionian

The Southern Ionian region has the biggest number of available profiles (Table 1). Regarding temperature, the model profiles show an increased underestimation at surface areas, whilst at underlying layers (50-200 m) the model presents a much more variable behaviour (similar to the Northern Ionian region) (Fig. 6C). Likewise, the comparison of the average profiles between the model and the Argo data (Fig. 6A), indicates a similar pattern to the Northern Ionian region i.e. a model underestimation at intermediate depths, which increases with depth.

In general, the model slightly overestimates salinity values at almost all depths apart from LIW layer which is here presented deeper (200–500 m) compared to the rest sub-domains (Fig. 6B, 6D). Nevertheless, the comparison of the average profiles shows a good representation of the salinity field from the sub-surface layers down to 850 m. Likewise, AW and LIW signals indicate a good agreement between model and in-situ datasets (Fig. 6B). Both surface and deeper waters show similarities with the Northern Ionian region regarding average salinity values. Surface layers are underestimated by the model, whilst deeper layers (>800 m) are overestimated in comparison to the average Argo profile (Fig. 6B).

In the Southern Ionian region, both Argo and model temperature STD is presented slightly larger than the Northern Ionian at intermediate depths. On the contrary, salinity's STD is significantly smaller at the same layers (Fig. 6A, 6B).

Hydrographic features

The in-situ profiles depicted interesting interannual hydrographic changes in the study area during the 5-years period (2008 – 2012). Focusing on the Northern Ionian and the water mass exchanges with the Adriatic Sea, the yearly Argo average salinity profiles have been produced in an attempt to investigate the interannual variability of the dominant water masses of the region (Fig. 7A, 7B). Under this examination, all the available profiles of the Northern Ionian were taken into account, whilst the Otranto Strait and Southern Adriatic sub-domains were merged (Table 1, Fig 1A). Nevertheless, only the years 2010 and 2012 are presented for that domain (SA & OS) since the available profiles were very few during 2009 and 2011. As shown from the *in-situ* profiles

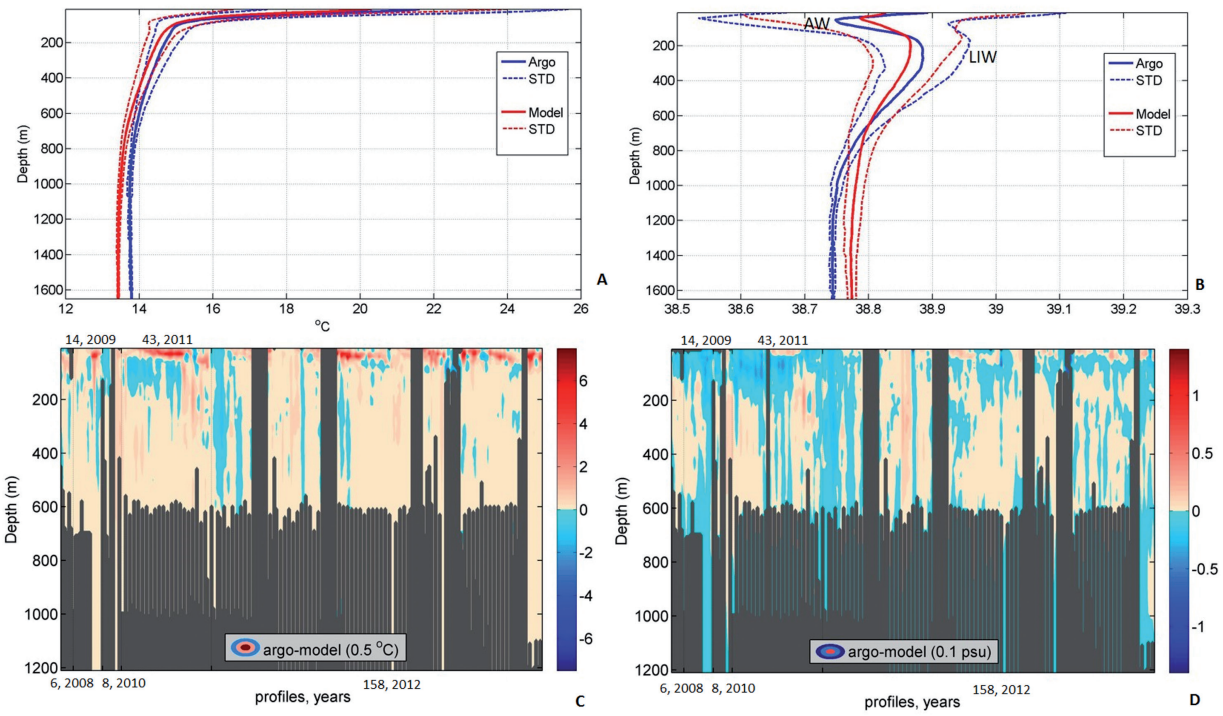

Fig. 5: Temperature (A) and salinity (B) average profiles with the associated STD for model (red) and Argo (blue), calculated from the available profiles in the northern Ionian region. Hovmöller diagrams of the differences between Argo and model associated profiles over time for temperature (C) and salinity (D) in the northern Ionian.

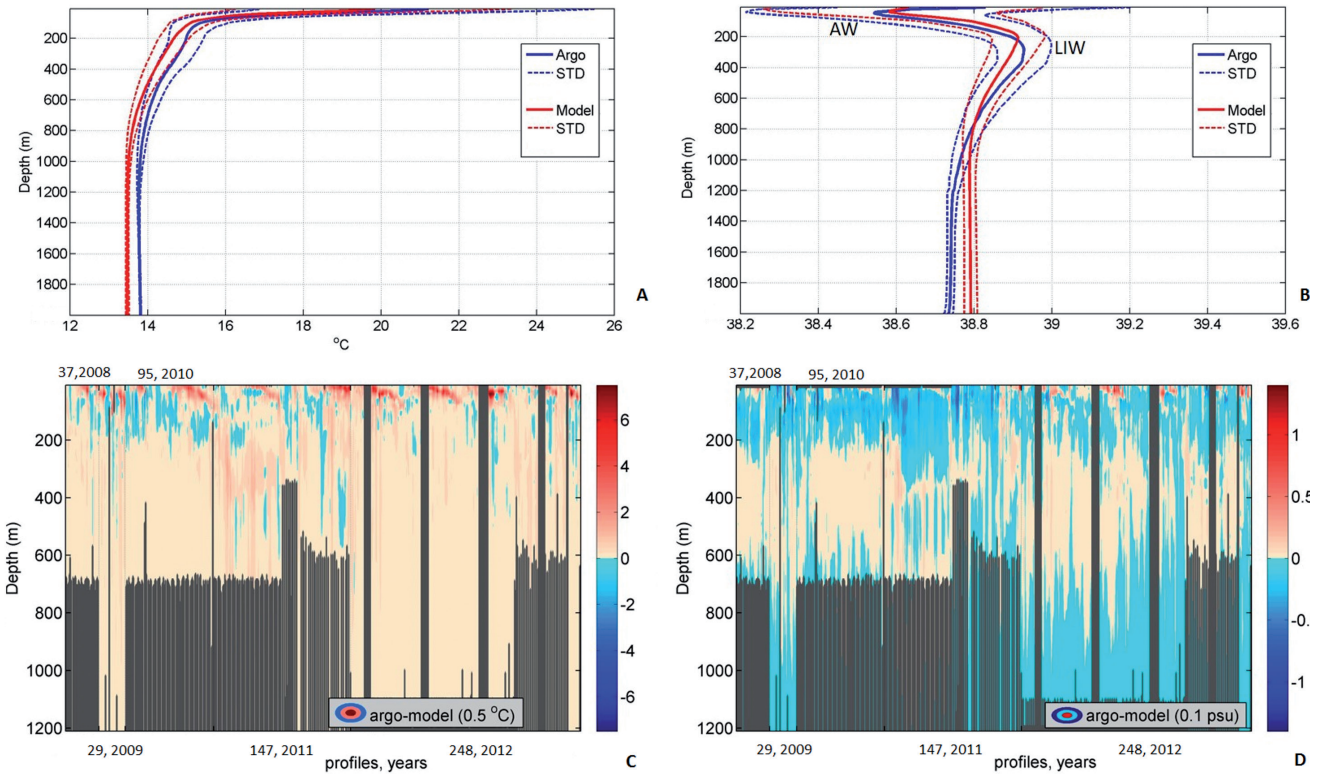

Fig. 6: Temperature (A) and salinity (B) average profiles with the associated STD for model (red) and Argo (blue), calculated from the available profiles in the southern Ionian region. Hovmöller diagrams of the differences between Argo and model associated profiles over time for temperature (C) and salinity (D) in the southern Ionian.

Table 1. Argo-Model associated profiles per year and geographical area SA: Southern Adriatic, OS: Otranto Strait, NI: Northern Ionian, SI: Southern Ionian. (Note: 17 profiles in the Taranto Bay have been excluded from the regional analysis)

Years/Region	SA	OS	NI	SI	Sum
2008			6	37	43
2009		5	14	29	48
2010	57	2	8	95	162
2011		5	43	147	195
2012	46	11	158	248	463
Total	103	23	229	556	911

in the Northern Ionian, a gradual increase of the salinity is observed during 2009 – 2011 at intermediate and upper layers resulting in the weakening of the AW signal (38.33 psu in 2009, 38.54 psu in 2011) and the strengthening of the LIW (38.84 psu in 2009, 38.94 psu in 2011) (Fig. 7B). In 2012 the LIW core disappears whilst the salt content in the upper layers increases significantly. This is probably associated with the reported reversion of the upper layers circulation from cyclonic in 2011 to anti-cyclonic in 2012 (Gačić *et al.,* 2014). Although the anti-cyclonic mode of the Northern Ionian Gyre (NIG) could act as a cut off mechanism for the LIW northward transfer along the eastern Ionian, the results of the cyclonic circulation during 2011 are prominent in the Adriatic. An uplifted LIW signal appears in 2012 (38.85 psu at 100 m) in contrast with 2010 when this was totally absent (Fig. 7A). The salinity average profiles from model simulations seem to follow this increase yet underestimating LIW core by 0.7 psu (Fig. 7C. 7D). In the Northern Ionian, model results depict the strengthening of the LIW in 2011 however its core is underestimated, shallower and less extended. Moreover, SANI's AW signal is fade and in general presented saltier, whilst salinity simulation of deep waters shows a small interannual variability which is not depicted in the Argo results (Fig. 7D).

Another case study was performed on the south-eastern Ionian part in order to associate the aforementioned interannual variability of the salt content with the input from the basin's southern boundaries. An area between 22° E - 22° E & 35° N - 38° N is chosen in order to observe the Aegean salt input (Fig. 8A). A gradual salinity increase of the intermediate layers is apparent from the Argo profiles during the years 2008 – 2011 (Fig. 8A). This is in agreement with previous studies that have presented increased salinity signals in the south-eastern Ionian from mooring timeseries, associating these masses with an outflow from the western Cretan Arcs within the same period (Kassis *et al.,* 2011; Velaoras *et al.,* 2013; Kassis *et al.,* 2013). A strong LIW during 2011 appears weakened in 2012, thus depicting a similar variability with the Northern Ionian part described previously. This is in agreement with the concept that especially during the cyclonic NIG mode (2011) the LIW core travels along the Hellenic Trench coastline to reach Northern Io-

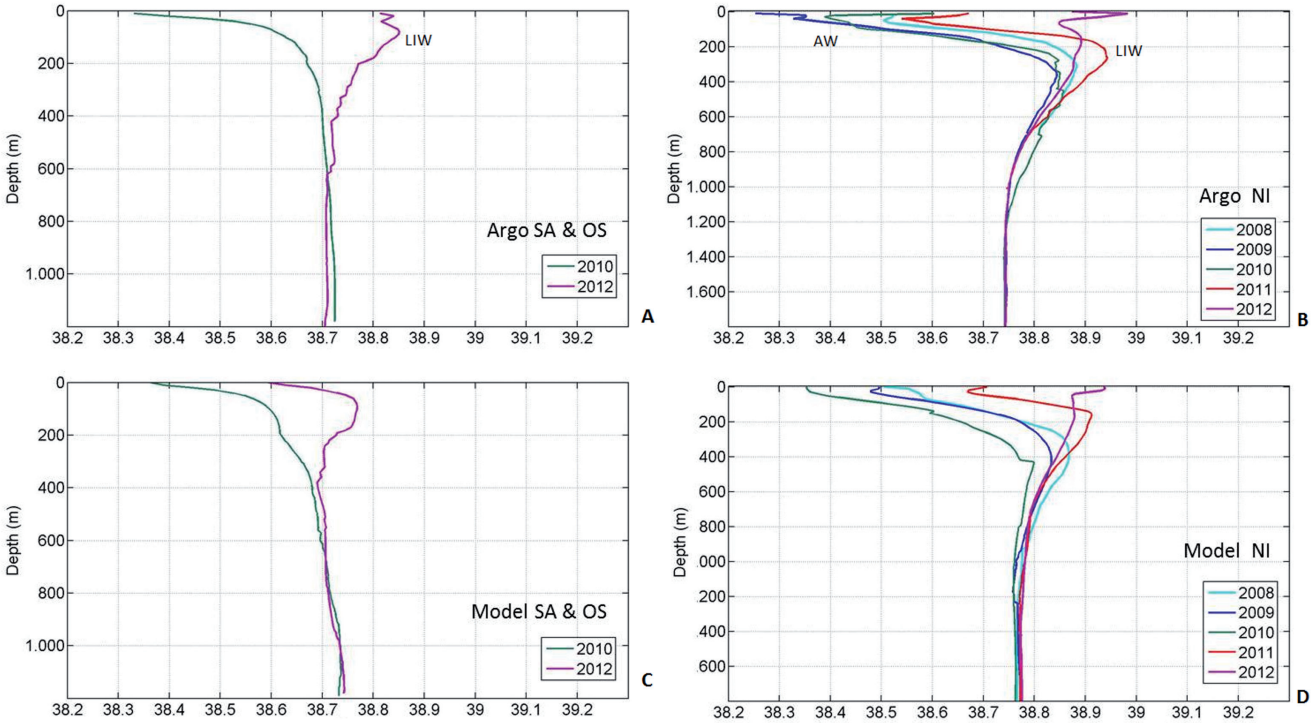

Fig. 7: **A:** Argo salinity average profiles in Southern Adriatic (SA) and Otranto Strait (OS) for the years 2010 (green) and 2012 (purple). **B:** Argo salinity average profiles in the Northern Ionian (NI) for the years 2008 (light blue), 2009 (dark blue), 2010 (green), 2011 (red) and 2012 (purple). **C:** Model salinity average profiles in Southern Adriatic (SA) and Otranto Strait (OS) for the years 2010 (green) and 2012 (purple). **D:** Argo salinity average profiles in the Northern Ionian (NI) for the years 2008 (light blue), 2009 (dark blue), 2010 (green), 2011 (red) and 2012 (purple).

nian's boundaries and eventually enter the Adriatic basin (Malanotte-Rizzoli *et al.,* 1997; Manca *et al.,* 2002; Gačić *et al.,* 2010). Regarding model simulations, although SANI fails to reproduce the intermediate layers salinity increase of 2010, the 2011 peak and 2012 weakening is simulated, but in shallower depth layers (< 200 m) (Fig. 8B). Likewise within the Northern Ionian, a salinity variability of the deep waters is also apparent in contrast with the Argo average profiles (Fig 8A, 8B).

Seasonal analysis

The seasonal averaged profiles (November - April and May - October), were derived from all available profiles in the euphotic zone (0 - 200 m), for each season. For temperature, the model appears to underestimate values from the surface layers down to 200 m for both seasons. During the cold periods of deep mixing (November – April), the surface temperature appears well correlated between the two datasets, whilst below surface model underestimation is shown that is increasing with depth to a maximum difference of 0.62 °C at 40 m (Fig. 9A). Contrastingly, for the warm periods of intense stratification (May – October), the averaged temperatures present significantly higher differences within the surface layer zone (1.30 °C at the surface, 1.82 °C at 20 m, and 1.23 °C at 40 m depth), after which they show a decrease with depth (Fig. 9B). The averaged salinity profiles for both seasons indicate that the model predicts saltier water at the surface with differences of 0.13 and 0.2 psu during the cold and warm periods respectively (Fig. 9C, 9D). Below the surface (10-20 m depth), the model fails to represent the salinity maximum depicted in the Argo profiles. This is particularly true for the warm period, where the model salinity average is depicted as 0.2 psu lower than the average Argo salinity (Fig. 9D). The salinity peak depicted at 10 m depth during the warm period is partially related to seasonal changes (reduced rainfall, river outputs etc.). Yet, it is also related to statistical reasons since the profiles of the warm period count 178 profiles more than the cold period. The majority of those come from 2011 & 2012 from NI & SI sub-domains where an increased sub-surface salinity has been observed (Fig. 7B, 8B). Nevertheless, in the layer 40 - 200 m the model presents less overestimation of the salt content during the warm period.

The calculated STD's for both periods do not present significant differences between Argo and model. However, the STDs of the warm period appear larger, especially at the surface layers (~ 3 °C , 0.4 psu at 20 m) in comparison to the cold period (~ 2.5 °C & 0.3 psu at 20 m), reflecting a higher seasonal variability (Fig. 9A, 9B, 9C, 9D).

General domain

Due to the majority of profiles (~80%) originating from NI and SI regions, the total averaged profiles

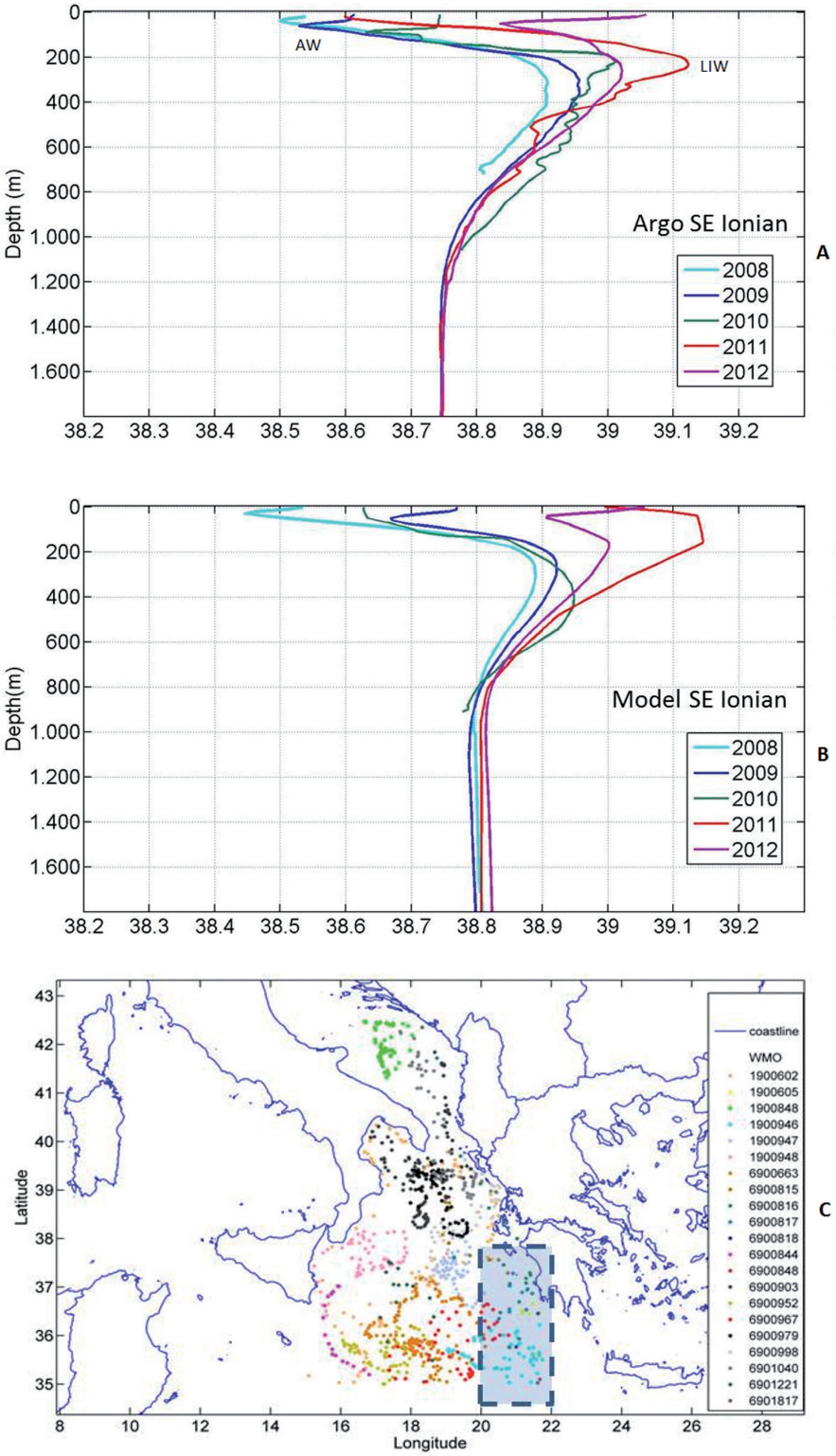

Fig. 8: **A:** Argo salinity average profiles in the south-eastern Ionian for the years 2008 (light blue), 2009 (dark blue), 2010 (green), 2011 (red) and 2012 (purple). **B:** Model salinity average profiles in the south-eastern Ionian for the years 2008 (light blue), 2009 (dark blue), 2010 (green), 2011 (red) and 2012 (purple).

naturally depict characteristics similar to these regions. The temperature average profiles indicate that the model constantly underestimates the heat content of the water column. The largest differences are notable at the surface layers with a maximum temperature difference of approximately 1.3 °C at 20 m depth whilst the minimum (~ 0.2 °C) occurs at 110 m depth. Below this depth and down to 1300 m the model's underestimation is consistently lower than 0.3 °C and gradually increases to reach 0.346 °C at 2000 m (Fig. 10A, 10B).

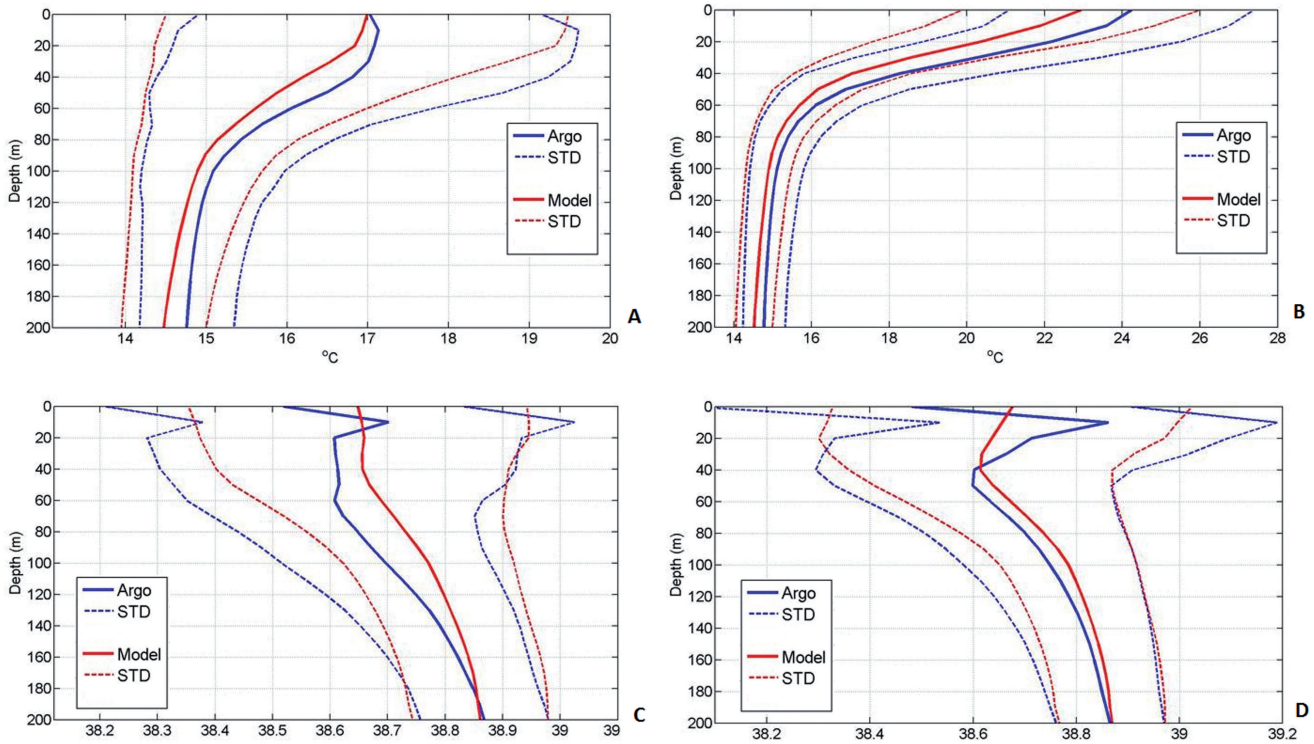

Fig. 9: Temperature (A) and salinity (C) average profiles with the associated STD for model (red) and Argo (blue), calculated from the associated profiles during the "winter" periods (November – April). The associated profiles for the "summer" periods (May – October) are shown in (B) and (D) for the temperature and salinity respectively.

According to the average salinity profiles the model underestimates surface waters by 0.14 psu (10 m depth), whilst overestimates salinity values in the layer between 30 and 200 m. Below 200 m, the model underestimates salinity values by approximately 0.02 - 0.03 psu and below 730 m fails to represent the gradual decrease of salinity values as is apparent from the in-situ average profiles. Due to this fact, a considerable difference of 0.05 psu is shown in the deep waters (Fig. 10B, 10C).

Although the model average profiles in both temperature and salinity seem to represent adequately the in-situ variability, the underestimation of the temperature field of intermediate and deep layers, results in the prediction of denser waters. The T-S diagram of the Argo and model profiles for the intermediate (200 - 800 m) and deep (800 – 2000 m) layers (Fig. 10D) visualizes these differences. Between 200 and 800 m, both datasets present similar distributions, with the model being characterized by slightly denser water masses. However, at deeper depths, the majority of the model T-S data shows much denser water masses (below the 29.2 kg m^{-3} σ_θ) than the in-situ data. This is mainly due to the temperature underestimation at these layers, as described previously, which is then translated into large differences in the density field (Fig. 10D). As shown in the Theta-S diagram (Fig. 10D) the deep waters simulated by the model (dark red dots) lie beneath the ones measured by Argo, whilst on the x-axis (salinity) the range of both datasets does not differ significantly. In order to quantify the T/S contribution on the density field simulated by the model, two case studies were carried out. For the 1st case we assume that the model simulates the same salinity field with Argo and therefore any difference on model's density can be attributed to its temperature underestimation. Contrariwise, for the 2nd case we assume that there is no difference in the temperature field of the two datasets and thus, the density differences can be attributed to the salinity overestimation by the model. The results confirm what is depicted in the Theta-S diagram. For the case 1, the Argo-model density differences are almost constant (~ 0.06 kg m^{-3}) below 800 m. On the contrary, in the 2nd case density differences are an order of magnitude less at 800 m and gradually increase with depth to reach approximately 0.038 kg m^{-3} at 2000 m.

The depth profiles of the Root Mean Square Errors (RMSE) for both temperature and salinity varies for the surface layers (Fig. 11A, 11C). In the first 50 m, RMSE reaches a maximum value for both parameters (1.9 at 30 m, and 0.21 at 20 m for temperature and salinity respectively) (Fig. 11A, 11C). This is also depicted in the profile vs. profile residuals of each parameter presented for 6 discrete depths. Positive residuals (Argo > model) are shown for temperature values, with maxima at the 30 - 40 m depth zone. Regarding salinity, the positive residuals are shown within the 20 - 40 m depth layer, whilst negative residuals are mainly present in the underlying zone (40 - 60 m) (Fig. 11B, 11D).

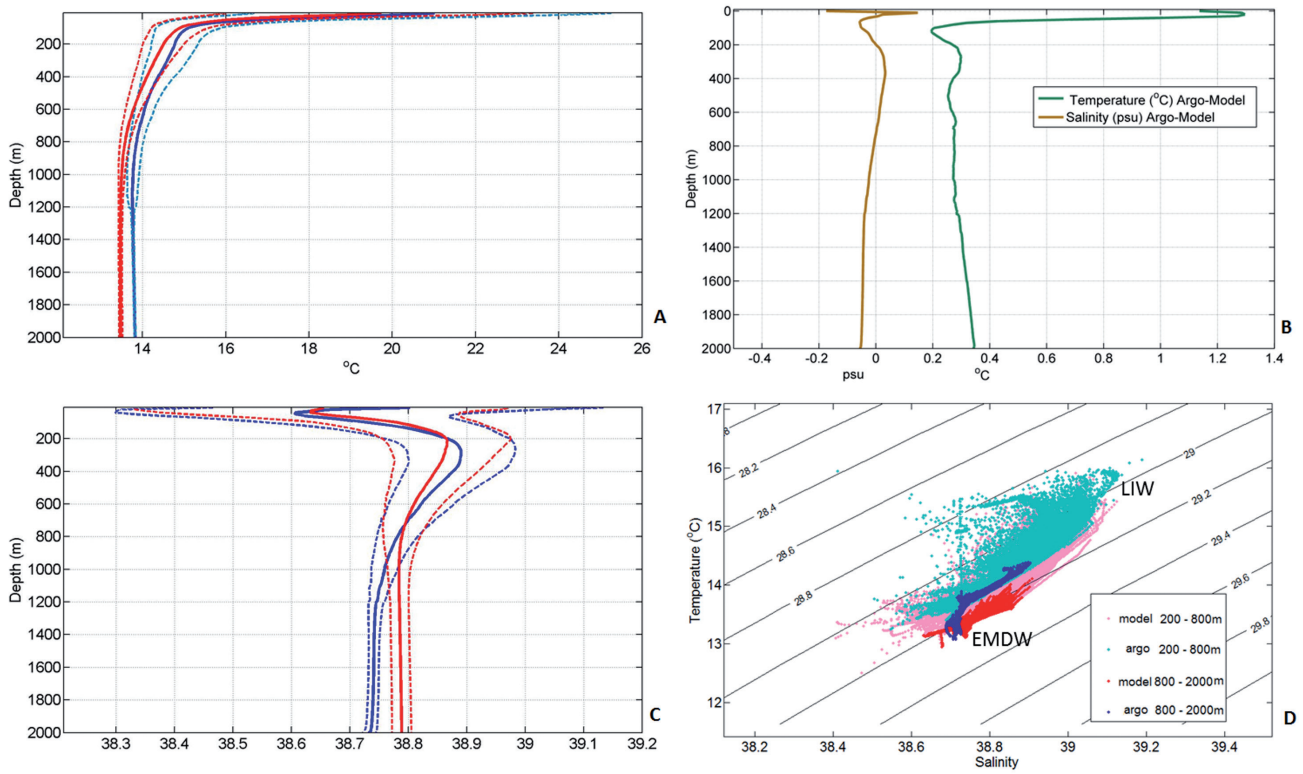

Fig. 10: Temperature (A) and salinity (C) average profiles with the associated STD for model (red) and Argo (blue), calculated from all the associated profiles of the study area (Fig. 1). Profile differences (Argo – model) of the average temperature (green line) and salinity (brown line) (B). T-S diagram of all Argo and model associated profiles for two depth layer zones (Argo: 200-800m light blue, 800-2000 m dark blue) (Model: 200-800 m pink, 800-2000 m red) (D).

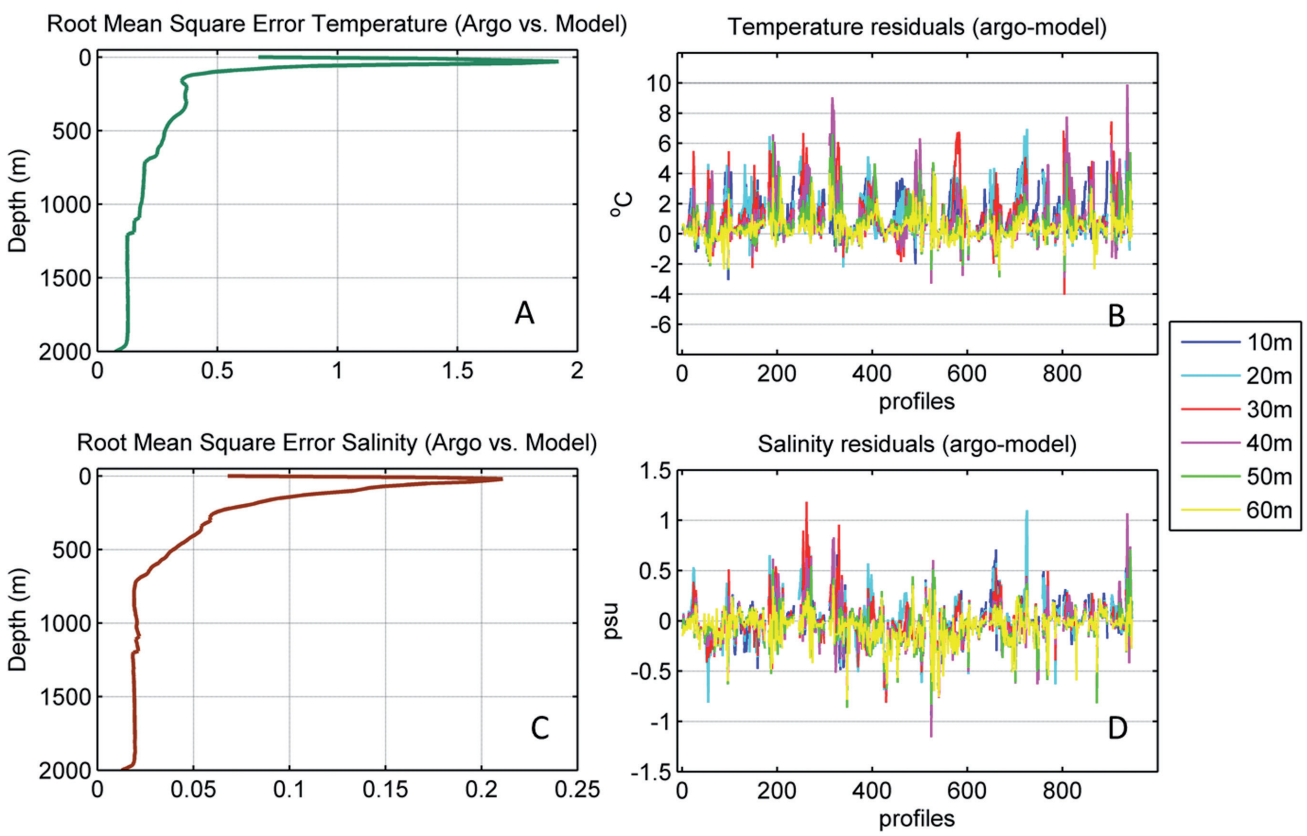

Fig. 11: RMSE profiles for temperature (A) and salinity (C). All associated profiles differences (Argo-model) for temperature (B) and salinity (D) in 6 discrete depths (10 m dark blue, 20 m light blue, 30 m red, 40 m pink, 50 m green, 60 m yellow).

Discussion

During the study period (2008 – 2012) the Ionian basin's hydrography has undergone changes associated with the general circulation of the wider area, meteorological conditions and water mass exchanges with its adjacent regions. Although modelling of such transitional areas is a difficult task, in this case the SANI model sufficiently represents the general hydrographic features of the Ionian Sea and Southern Adriatic water column. There are however, certain misrepresentations in both temperature and salinity fields within the wider area. The average temperature simulated by SANI is lower than the in-situ for the whole water column although greater differences are depicted at the surface layers. Although the model is able to reproduce the large scale anomalies of SST and an important part of sub-basin and mesoscale variability it presents a systematic underestimation of surface and near surface temperature with respect to ARGO floats measurements. We argue that such behavior calls for further tuning of the surface heat fluxes parameterization scheme used by the modelling system. Important differences are also shown for the deep waters, where the model systematically underestimates temperature. Regarding salinity, the model also underestimates near the surface, and at intermediate layers, whilst predicting saltier values for the sub-surface and deep waters. The latter, in conjunction with temperature underestimation, results in the prediction of particularly denser waters at the deeper layers of the study area. A quantification of T/S contribution regarding this overestimation showed that approximately 60% (2000 m) to 95% (800 m) of that difference is attributed to the temperature underestimation from SANI. The RMSE is considerably high within the first 50 m for both parameters. As shown from the seasonal analysis, the large differences in this layer mainly derive from the misrepresentation of the well-stratified upper layer that starts from late spring and ends in the early autumn period. The inter-annual changes in the wider area also affect SANI's performance as shown in the previous regional analysis. Especially for the Otranto Strait there is a clear shift in the profile to profile salinity and temperature differences for the years 2010 and 2012, where SANI generally underestimates both. In general there is a tendency of an underestimation of salinity at intermediate layers from the model during the years 2010 and 2012, which is apparent in all regions. This is probably associated with the inter-annual hydrodynamic changes in the area as described previously.

Next steps of SANI improvement

Regarding the modelling system itself, two major upgrades have been put forward: the first chunk involves a data assimilation system that has been already developed and tested with very promising results due to the Greek national KRIPIS project. The assimilation system is based on a localized version of SEEK filter (Korres *et al.,* 2014) and operates on a weekly basis using all available in-situ (Argo profiles and XBT's) and satellite (absolute dynamic topography and SST) observations in the Ionian – Southern Adriatic area. The innovation of the system lies in the fact that the model analysis is treated by the VIFOP package in order to damp velocity divergence due to updates introduced during the analysis phase. The second chunk of upgrade involves the one-way coupling of the hydrodynamics with the wind-waves in terms of wave dissipated energy insertion into the vertical mixing scheme of the model (Breivik *et al.,* 2015) and the stokes drift velocity inclusion into the Navier-Stokes equations following Bennis *et al.,* (2011) approach. At the same time a fine tuning of the surface heat fluxes parameterization scheme will take place in order to decrease the negative bias of the model surface temperature with respect to Argo measurements and SST satellite retrievals.

Conclusions

Regarding the analysis performed in the area's hydrography from the averaged profiles, the following conclusions can be summarized in regards to the characteristic water masses and the model's performance:

– A salt increase at intermediate and upper layers has been observed from 2008 until 2011 in the Ionian basin. This increase is most prominent in its south-eastern part but is also apparent in its northern region.

– More specifically, strong signals of LIW are observed from the south to the north during 2011 when the NIG has been reported as cyclonic. This is probably associated with an increased LIW inflow from the south that travels northward until Adriatic.

– At the same time, the AW inflow in the Ionian is gradually reduced reaching a minimum in 2012 in all sub-domains.

– Although sea surface salinity from Argo is sparse, the data of the first 10 m depicts the model's underestimation of the LSW and ISW regarding salt.

– The AW core is represented as shallower, slightly saltier and colder in the model simulation (30 - 40 m, 38.63 psu, 17.18^{o} C) compared with the Argo data (40 - 50 m, 38.61 psu, 17.20^{o} C).

– LIW is also underestimated for both T/S by the model. SANI outputs depict a salinity maximum of 38.87 psu and temperature 14.49^{o} C at 210 m whilst the Argo profiles show a salinity maximum of 38.89 psu and temperature 14.63^{o} C at 280 m.

– Both temperature and salinity fields of deep intermediate water masses show in general good representation from SANI.

– Water masses that occupy the deep layers of the Ionian are simulated denser by the SANI model, mainly due to a gradually increasing temperature underestimation with depth below 800 m.

In general the SANI example has shown that high resolution model simulations in marginal seas are promising. Nevertheless, the upgrade and expansion, both in new sensors and coverage, of the in-situ observing platforms, will play a key role for the assessment of the models' performance in such areas.

Acknowledgements

This work has been supported by the "Greek Research Infrastructure for Observing the Oceans – GREEK ARGO" project (ERDF 2007-2013) and the IONIO Interreg-III project funded by the European Territorial Cooperation Operational Programme "Greece-Italy" (2007 – 2013).

References

Auclair, F., Estournel, C., Marsaleix, P., Pairaud, I., 2006. On coastal ocean embedded modeling. *Geophysical Research Letters*, 33 (14), L14602.

Bennis, A.-C., Ardhuin, F., Dumas, F., 2011. On the coupling of wave and three-dimensional circulation models: Choice of theoretical framework, practical implementation and adiabatic tests. *Ocean Modelling*, 40 (3-4), 260-272.

Bensi, M., Rubino, A., Cardin, V., Hainbucher, D., Mancero-Mosquera, I., 2013. Structure and variability of the abyssal water masses in the Ionian Sea in the period 2003-2010. *Journal of Geophysical Research: Oceans*, 118 (2), 931-943.

Bessières, L., Rio, M.H., Dufau, C., Boone, C., Pujol, M.I., 2013. Ocean state indicators from MyOcean altimeter products. *Ocean Sci.*, 9 (3), 545-560.

Borzelli, G.L.E., Gačić, M., Cardin, V., Civitarese, G., 2009. Eastern Mediterranean Transient and reversal of the Ionian Sea circulation. *Geophysical Research Letters*, 36 (15), L15108.

Breivik, Ø., Mogensen, K., Bidlot, J.-R., Balmaseda, M.A., Janssen, P.A.E.M., 2015. Surface wave effects in the NEMO ocean model: Forced and coupled experiments. *Journal of Geophysical Research: Oceans*, 120 (4), 2973-2992.

Cardin, V., Civitarese, G., Hainbucher, D., Bensi, M., Rubino, A., 2015. Thermohaline properties in the Eastern Mediterranean in the last three decades: is the basin returning to the pre-EMT situation? *Ocean Science*, 11 (1), 53-66.

Gačić, M., Kovacevic, V., Manca, B., Papageorgiou, E., Poulain, P. *et al.*, 1996. Thermohaline properties and circulation in the Otranto Strait. *Bulletin-Institut Oceanographique Monaco-Numero Special-*, 117-146.

Gačić, M., Borzelli, G.L.E., Civitarese, G., Cardin, V., Yari, S., 2010. Can internal processes sustain reversals of the ocean upper circulation? The Ionian Sea example. *Geophysical Research Letters*, 37 (9), L09608.

Gačić, M., Civitarese, G., Kovačević, V., Ursella, L., Bensi, M. *et al*., 2014. Extreme winter 2012 in the Adriatic: an example of climatic effect on the BiOS rhythm. *Ocean Science*, 10 (3), 513-522.

Hainbucher, D., Rubino, A., Cardin, V., Tanhua, T., Schroeder, K. *et al*., 2014. Hydrographic situation during cruise M84/3 and P414 (spring 2011) in the Mediterranean Sea. *Ocean Science*, 10 (4), 669-682.

Hellerman, S., Rosenstein, M., 1983. Normal Monthly Wind Stress Over the World Ocean with Error Estimates. *Journal of Physical Oceanography*, 13 (7), 1093-1104.

Jerlov, N.G., 1976. *Marine optics*, 231 pp. Elsevier Oceanography Series, (14).

Kassis, D., Nittis, K., Perivoliotis, L., Chondronasios, A., Petihakis, G. *et al*., 2011. Hydrodynamic properties of the south Ionian Sea based on the POSEIDON Pylos observatory. In Proceedings of the 6th international conference on EuroGOOS. eds. H. Dahlin, NC Flemming and S. Petersson. EuroGOOS Publication. pp. 59-66.

Kassis, D., Nittis, K., Perivoliotis, L., 2013. Hydrodynamic variability based on the multi-parametric POSEIDON Pylos observatory of the south Ionian Sea. *Ocean Science Discussions*, 10 (3), 883-921.

Kassis, D., Korres, G., Petihakis, G., Perivoliotis, L., 2015. Hydrodynamic variability of the Cretan Sea derived from Argo float profiles and multi-parametric buoy measurements during 2010–2012. *Ocean Dynamics*, 65 (12), 1585–1601.

Klein, B., Roether, W., Manca, B.B., Bregant, D., Beitzel, V. *et al*., 1999. The large deep water transient in the Eastern Mediterranean. *Deep Sea Research Part I: Oceanographic Research Papers*, 46 (3), 371-414.

Klein, B., Roether, W., Manca, B., Theocharis, A., 2000. The evolution of the Eastern Mediterranean Climatic transient during the last decade: the tracer viewpoint. In *In The Eastern Mediterranean Transient,* edited by: Briand, F., CIESM Workshop Series, vol. 10, pp. 21-25. 2000. pp. 21-25.

Korres, G., Lascaratos, A., 2003. A one-way nested eddy resolving model of the Aegean and Levantine basins: implementation and climatological runs. *Annales Geophysicae*, 21 (1), 205-220.

Korres, G., Nittis, K., Hoteit, I., Triantafyllou, G., 2009. A high resolution data assimilation system for the Aegean Sea hydrodynamics. *Journal of Marine Systems*, 77 (3), 325-340.

Korres, G., Ntoumas, M., Potiris, M., Petihakis, G., 2014. Assimilating Ferry Box data into the Aegean Sea model. *Journal of Marine Systems*, 140, Part A, 59-72.

Krokos, G., Aarts, G., Velaoras, D., Korres, G., Perivoliotis, L. *et al*., 2014. On the continuous functioning of an internal mechanism that drives the Eastern Mediterranean thermohaline circulation: The recent activation of the Aegean Sea as a dense water source area. *Journal of Marine Systems*, 129, 484-489.

Ludwig, W., 2007. River inputs to Southern European seas: Major drivers for ecosystem changes during past and future decades. p. 29. In *38th CIESM Congress Proceedings*. CIESM_Congress,_Istanbul, 2007.

Lykousis, V., Nittis, K., Ballas, D., Perivoliotis, L., Kassis, D. *et al*., 2015. The Hellenic deep sea observatory: Science objectives and implementation. In *SEA FLOOR OBSERVATORIES*. Springer Praxis Books. Springer Berlin Heidelberg, pp. 81-103.

Malanotte-Rizzoli, P., Manca, B.B., D'Alcalà, M.R., Theocharis, A., Bergamasco, A. *et al*., 1997. A synthesis of the Ionian Sea hydrography, circulation and water mass pathways during POEM-Phase I. *Progress in Oceanography*, 39 (3), 153-204.

Manca, B.B., Kovaĉević, V., Gaĉić, M., Viezzoli, D., 2002. Dense water formation in the Southern Adriatic Sea and spreading into the Ionian Sea in the period 1997-1999. *Journal of Marine Systems*, 33–34, 133-154.

Meccia, V.L., Borghini, M., Sparnocchia, S., 2015. Abyssal circulation and hydrographic conditions in the Western Ionian Sea during Spring–Summer 2007 and Autumn–Winter 2007–2008. *Deep Sea Research Part I: Oceanographic Research Papers*, 104, 26-40.

Mellor, G.L., Yamada, T., 1982. Development of a turbulence closure model for geophysical fluid problems. *Reviews of Geophysics*, 20 (4), 851–875.

Nittis, K., Pinardi, N., Lascaratos, A., 1993a. Characteristics of the summer 1987 flow field in the Ionian Sea. *Journal of Geophysical Research: Oceans*, 98 (C6), 10171-10184.

Nittis, K., Pinardi, N., Lascaratos, A., 1993b. Characteristics of the summer 1987 flow field in the Ionian Sea. *Journal of Geophysical Research: Oceans*, 98 (C6), 10171-10184.

Nittis, K., Perivoliotis, L., Korres, G., Tziavos, C., Thanos, I., 2006. Operational monitoring and forecasting for marine environmental applications in the Aegean Sea. *Environmental Modelling & Software*, 21 (2), 243-257.

Oddo, P., Adani, M., Pinardi, N., Fratianni, C., Tonani, M. *et al*., 2009. A nested Atlantic-Mediterranean Sea general circulation model for operational forecasting. *Ocean Sci.*, 5 (4), 461-473.

Papadopoulos, A., Katsafados, P., 2009. Verification of operational weather forecasts from the POSEIDON system across the Eastern Mediterranean. *Natural Hazards and Earth System Sciences*, 9 (4), 1299-1306.

Pinardi, N., Zavatarelli, M., Adani, M., Coppini, G., Fratianni, C. *et al*., 2015. Mediterranean Sea large-scale low-frequency ocean variability and water mass formation rates from 1987 to 2007: A retrospective analysis. *Progress in Oceanography*, 132, 318-332.

Poulain, P., Barbanti, R., Font, J., Cruzado, A., Millot, C. *et al*.,, 2007. MedArgo: a drifting profiler program in the Mediterranean Sea. *Ocean Science*, 3 (3), 379-395.

Roether, W., Schlitzer, R., 1991. The Mediterranean Sea Eastern Mediterranean deep water renewal on the basis of chlorofluoromethane and tritium data. *Dynamics of Atmospheres and Oceans*, 15 (3), 333-354.

Roether, W., Manca, B.B., Klein, B., Bregant, D., Georgopoulos, D. *et al*., 1996. Recent Changes in Eastern Mediterranean Deep Waters. *Science*, 271 (5247), 333-335.

Schroeder, K., Millot, C., Bengara, L., Ben Ismail, S., Bensi, M. *et al*., 2013. Long-term monitoring programme of the hydrological variability in the Mediterranean Sea: a first overview of the HYDROCHANGES network. *Ocean Science*, 9 (2), 301-324.

Theocharis, A., Georgopoulos, D., Lascaratos, A., Nittis, K., 1993. Water masses and circulation in the central region of the Eastern Mediterranean: Eastern Ionian, South Aegean and Northwest Levantine, 1986–1987. *Deep Sea Research Part II: Topical Studies in Oceanography*, 40 (6), 1121-1142.

Theocharis, A., Klein, B., Nittis, K., Roether, W., 2002. Evolution and status of the Eastern Mediterranean Transient (1997–1999). *Journal of Marine Systems*, 33-34, 91-116.

Theocharis, A., Krokos, G., Velaoras, D., Korres, G., 2014. An Internal Mechanism Driving the Alternation of the Eastern Mediterranean Dense/Deep Water Sources. In G. L. E. Borzelli, M. Gačić, P. Lionello, & Malanotte-Rizzoli, P. (Eds). *The Mediterranean Sea*. John Wiley & Sons, Inc., pp. 113-137. Available at: http://onlinelibrary.wiley.com/doi/10.1002/9781118847572.ch8/summary [Accessed March 8, 2016].

Tonani, M., Oddo, P., Korres, G., Clementi, E., Dobricic, S. *et al*., 2014. The Mediterranean Forecasting System: recent developments. In EGU General Assembly Conference Abstracts. p. 16899.

Velaoras, D., Kassis, D., Perivoliotis, L., Pagonis, P., Hondronasios, A. *et al*., 2013. Temperature and salinity variability in the Greek Seas based on POSEIDON stations time series: preliminary results. *Mediterranean Marine Science*, 14 (3), 5-18.